

# ESO Imaging Survey

## Deep Public Survey: Infrared Data for the Chandra Deep Field South\*.

B. Vandame<sup>1</sup>, L.F. Olsen<sup>2</sup>, H.E. Jørgensen<sup>2</sup>, M.A.T. Groenewegen<sup>1</sup>, M. Schirmer<sup>1,3</sup>, S. Arnouts<sup>1</sup>, C. Benoist<sup>4,1</sup>, L. da Costa<sup>1</sup>, R. P. Mignani<sup>1</sup>, C. Rit <sup>1,5</sup>, R. Slijkhuis<sup>1</sup>, E. Hatziminaoglou<sup>1</sup>, R. Hook<sup>1</sup>, R. Madejsky<sup>1</sup>, and A. Wicenec<sup>1</sup>

<sup>1</sup> European Southern Observatory, Karl-Schwarzschild-Str. 2, D-85748 Garching b. M nchen, Germany

<sup>2</sup> Astronomical Observatory, Juliane Maries Vej 30, DK-2100 Copenhagen, Denmark

<sup>3</sup> Max-Planck Institut f r Astrophysik, Karl-Schwarzschild-Str. 1, D-85748 Garching b. M nchen, Germany

<sup>4</sup> Observatoire de la C te d'Azur, BP 229, 06304 NICE cedex 4, France

<sup>5</sup> Observat rio Nacional, Rua Gen. Jos  Cristino 77, Rio de Janeiro, R.J., Brasil

Received ; accepted

**Abstract.** This paper presents new  $J$  and  $K_s$  near-infrared data obtained from observations of the Chandra Deep Field South (CDF-S) conducted at the ESO 3.5m New Technology Telescope (NTT). These data were taken as part of the ongoing Deep Public Survey (DPS) being carried out by the ESO Imaging Survey (EIS) program, extending the EIS-DEEP survey. Combined these surveys now provide a contiguous coverage over an area of 400 square arcmin in the near-infrared, nearly matching that covered by the deep X-ray observations of Chandra, four times the area of the original EIS-DEEP survey. The paper briefly describes the observations and the new techniques being employed for pipeline processing jittered infrared observations, which include unbiased de-fringing and sky-background subtraction, pixel-based astrometry and stacking and pixel registration based on a multi-resolution decomposition of the images. The astrometric solution is based on a pre-release of the GSC-II catalog and has an accuracy of  $\lesssim 0.15$  arcsec. The final images for 12 pointings presented here reach median  $5\sigma$  limiting magnitudes of  $J_{AB} \sim 23.4$  and  $K_{AB} \sim 22.6$  as measured within an aperture  $2 \times \text{FWHM}$ . The frame to frame variation of the photometric zero-point is estimated to be  $\lesssim 0.09$  mag. The data are publicly available in the form of fully calibrated  $J$  and  $K_s$  pixel maps and source lists extracted for each pointing. These data can be requested through the URL “<http://www.eso.org/eis>”.

**Key words.** catalogs – surveys – stars: general - galaxies: general

## 1. Introduction

Deep multi-wavelength observations of selected regions of the sky from space and ground-based facilities, combined with spectrographic observations from large-aperture telescopes, offer the most promising means to probe the distant universe and study in a comprehensive way the evolution of galaxies and large-scale structures over a broad interval of look-back time. Preliminary steps towards this goal are already underway with the completion of deep X-ray observations of the Chandra Deep Field South (CDF-S;  $\alpha = 03^h32^m28^s$  and  $\delta = -27^\circ48'30''$ ; Giacconi *et al.* 2000). These observations will eventually be complemented by observations with HST, XMM and SIRTf as well as VLT.

Foreseeing the need for ground-based multi-color data the Working Group for public surveys at ESO recommended the ESO Imaging Survey (EIS, Renzini & da Costa, 1997) project to undertake deep, optical/infrared observations of the HDF-S

and CDF-S regions. Original observations of these fields were conducted in 1998 (da Costa *et al.* 1998; Rengelink *et al.* 1998, to be superseded by da Costa *et al.* 2001; Benoist *et al.* 2001a) and fully calibrated images, source catalogs and high-redshift galaxy candidates were immediately made public prior to the Science Verification of the first unit of the VLT. However, these observations covered only a small fraction of the field of view of Chandra, requiring the original coverage of EIS to be enlarged. Full coverage of the CDF-S  $\lesssim 350$  square arcmin field and flanking regions in optical and infrared is one of the primary goals of the Deep Public Survey (DPS) now being conducted by EIS. DPS consists of two parts: first, a deep, optical multi-passband ( $UBVRI$ ) survey reaching limiting magnitudes  $m_{AB} \sim 26$  mag covering three distinct strips (DEEP1, DEEP2 and DEEP3). These stripes consist of four adjacent pointings (denoted by a-d in decreasing order of right ascension) of the wide-field imager (WFI), mounted on the ESO/MPG 2.2m telescope at La Silla, yielding an area of one square degree each; second, the contiguous coverage in the infrared passbands  $JK_s$  of two distinct regions (DEEP-2c and DEEP-3a) 450 square arcmin each. The infrared part of DPS is a joint effort between

Send offprint requests to: [bvandame@eso.org](mailto:bvandame@eso.org)

\* Based on observations collected at the European Southern Observatory, La Silla, Chile within program ESO 164.O-0561.

the EIS team and an external group of scientist from ESO member states. Further details about DPS can be found at the URL "http://www.eso.org/eis". The primary goal of the survey is to produce a data set from which statistical samples of galaxies can be drawn to study the large scale structures at high redshift. These data should also be valuable for many other areas of investigation, in particular for cross-identification with X-ray sources detected from the deep X-ray exposure of Chandra.

The purpose of the present paper is to describe and present the data from the new infrared observations of the CDF-S region. The data reported here complement those obtained by the original EIS-DEEP survey (Rengelink *et al.* 1998), which are being re-analyzed and will be presented in a separate paper (Benoist *et al.* 2001a). Section 2 reviews the overall observing strategy and describes the observations. Section 3 discusses the techniques employed in the data reduction and the photometric and astrometric calibration of the images. Section 4 presents the photometric parameters of the sources detected on each image corresponding to different pointings and passband. Due to time constraints other products such as image mosaics, catalogs extracted from them, optical/infrared color catalogs, statistical samples and lists containing other targets of potential interest will be presented elsewhere. Even though the goal of the present paper is not to interpret the data, Section 5 presents the results of comparisons between the present observations and those of other authors. This is done for the sole purpose of assessing the quality of the astrometry and photometry of the present data set. Finally, a brief summary is presented in Section 6.

## 2. Observations

Infrared observations in the near-infrared passbands  $J$  and  $K_s$  were obtained using the SOFI camera (Moorwood, Cuby & Lidman 1998) mounted on the New Technology Telescope (NTT) at La Silla. SOFI is equipped with a Rockwell 1024<sup>2</sup> detector that, when used together with its large field objective, provides images with a pixel scale of 0.29 arcsec, and a field of view of about  $4.9 \times 4.9$  square arcmin. The infrared pointings were chosen to produce a contiguous coverage of a  $4 \times 4$  mosaic when combined with those of EIS-DEEP. They were also required to produce sufficient overlap between adjacent pointings to enable the construction of an image mosaic, avoiding severe decrease in the effective exposure time due to the jitter pattern used and enabling a common photometric zero-point to be determined. The inner  $2 \times 2$  subset correspond to the EIS-DEEP pointings reported by Benoist *et al.* (2001a). The remaining 12 pointings are those observed as part of the present survey which are listed in Table 1. The table gives: in column (1) the identification of each tile in the mosaic represented by the indices  $(i, j)$ , where  $i$  decreases with declination and  $j$  decreases with right ascension; and in columns (2) and (3) the J2000 coordinates of the pointing. A schematic view of the coverage is illustrated in Figure 1 which shows the relative positions of the region with  $UBVRI$  coverage, the EIS-DEEP infrared data and the newly accumulated data. In the convention described above the pointings with (2,2) (2,3), (3,2) and (3,3), correspond to those obtained by the EIS-DEEP program.

**Table 1.** Central position of the 12 SOFI fields observed as part of the DPS infrared survey of CDF-S (DEEP2c).

$(i, j)$	$\alpha$ (J2000)	$\delta$ (J2000)
(1,1)	03 <sup>h</sup> 32 <sup>m</sup> 57 <sup>s</sup>	-27°41'45"
(1,2)	03 <sup>h</sup> 32 <sup>m</sup> 37 <sup>s</sup>	-27°41'45"
(1,3)	03 <sup>h</sup> 32 <sup>m</sup> 17 <sup>s</sup>	-27°41'45"
(1,4)	03 <sup>h</sup> 31 <sup>m</sup> 57 <sup>s</sup>	-27°41'45"
(2,1)	03 <sup>h</sup> 32 <sup>m</sup> 57 <sup>s</sup>	-27°46'10"
(2,4)	03 <sup>h</sup> 31 <sup>m</sup> 57 <sup>s</sup>	-27°46'10"
(3,1)	03 <sup>h</sup> 32 <sup>m</sup> 57 <sup>s</sup>	-27°50'35"
(3,4)	03 <sup>h</sup> 31 <sup>m</sup> 57 <sup>s</sup>	-27°50'35"
(4,1)	03 <sup>h</sup> 32 <sup>m</sup> 57 <sup>s</sup>	-27°55'00"
(4,2)	03 <sup>h</sup> 32 <sup>m</sup> 37 <sup>s</sup>	-27°55'00"
(4,3)	03 <sup>h</sup> 32 <sup>m</sup> 17 <sup>s</sup>	-27°55'00"
(4,4)	03 <sup>h</sup> 31 <sup>m</sup> 57 <sup>s</sup>	-27°55'00"

The original goal of the observations was to reach  $5\sigma$  magnitudes of  $J_{AB}=23.5$  and  $K_{AB}=23.1$  requiring a total integration time of 1800 sec and 7000 sec in  $J$  and  $K_s$ , respectively, as estimated from the SOFI exposure time calculator. Following a Working Group (WG) recommendation, the total integration time of 8400 sec was later split into 3600 sec in  $J$  and 4800 sec in  $K_s$  to reach  $(J - K_s) \sim 2$  (Vega system) at the limiting magnitude of the survey. The  $J$  exposures were taken as a sequence of 60 one-minute exposures, while the  $K_s$  observations were split into two sequences of 40 one-minute exposures. However, during the reductions images with very high noise level and/or unexplained gradients in the background were detected and rejected from further processing. Therefore, in some cases the effective exposure time may vary with respect to those originally planned (see Section 5). In other cases, additional exposures were obtained for a pointing. These additional exposures typically originate from aborted exposure sequences, which were later re-observed in their entirety.

A total of 16 nights were allocated to the infrared part of DPS split into three runs: one in period 64 and two in period 66. The observations was carried out for both the DEEP2c and the DEEP3a regions, and a summary of the observations carried out in the DEEP2c region is given in Table 2, which lists: in column (1) the date of the observations; in column (2) the pointing as defined above; in column (3) the filters used; and in columns (4) and (5) the range and average seeing during the night as measured by the seeing monitor at La Silla. The observations were conducted under fairly good weather and seeing ( $\lesssim 1.1$  arcsec) conditions, nearly all in photometric nights, except for occasional light cirrus. Unfortunately, the last run was cancelled due to technical problems with the NTT. At the time of writing the  $J$  pointing (4,4) had been observed in service mode and will be made available as soon as possible.

The infrared observations were jittered relative to the centers given above in order to estimate the sky level from the data themselves. The procedure consists of a series of short exposures with small position offsets from the target position. The jitter strategy has been implemented as a standard observing template (AutoJitter) for the SOFI instrument. Each exposure consisted of the average of six ten-second sub-exposures.

**Fig. 1.** Relative positions of the area with *UBVRI* coverage (outer square) and the infrared data from EIS-DEEP (inner bright square) and the current survey. It can be seen that the infrared data forms a contiguous mosaic covering a significant fraction of the optical survey area. It also nearly coincides with the area covered by the deep observations of Chandra.

**Table 2.** Log of the observations for the infrared data for DEEP2c.

Date	Pointing (i,j)	Filter	Seeing range (arcsec)	Mean seeing (arcsec)
31-01-2000	(1,3)	$K_s$	–	–
01-02-2000	(1,3)	$K_s$	–	–
	(1,2)	$K_s$	0.66 – 1.07	0.90
03-02-2000	(1,3)	$J$	0.79 – 1.35	0.97
	(1,2)	$K_s$	0.60 – 0.92	0.76
04-02-2000	(1,2)	$J$	0.68 – 1.37	0.91
	(4,3)	$K_s$	0.69 – 1.17	0.87
05-02-2000	(4,3)	$J$	0.44 – 0.83	0.60
06-02-2000	(4,3)	$K_s$	0.43 – 0.63	0.52
19-11-2000	(4,2)	$K_s$	0.70 – 1.00	0.83
	(4,2)	$J$	0.68 – 1.17	0.85
	(1,1)	$J$	0.70 – 2.26	1.14
	(1,1)	$K_s$	0.56 – 2.07	0.95
20-11-2000	(1,1)	$K_s$	0.54 – 0.96	0.75
	(2,1)	$K_s$	0.54 – 1.01	0.77
	(2,1)	$J$	0.61 – 1.04	0.79
	(3,1)	$J$	0.63 – 1.17	0.81
	(3,1)	$K_s$	0.69 – 1.71	1.10
21-11-2000	(4,1)	$K_s$	0.56 – 1.11	0.82
	(1,4)	$K_s$	0.64 – 1.33	0.87
	(4,1)	$J$	0.60 – 1.98	1.16
	(1,4)	$J$	0.54 – 1.58	0.80
	(2,4)	$K_s$	0.72 – 1.52	1.01
22-11-2000	(2,4)	$K_s$	0.50 – 1.19	0.79
	(2,4)	$J$	0.60 – 2.40	1.14
	(3,4)	$K_s$	0.57 – 1.26	1.00
	(3,4)	$J$	0.62 – 1.49	0.94
	(4,4)	$K_s$	0.53 – 0.86	0.68

Using this template, offsets are generated randomly within a square box of a specified size, chosen originally to be 40 arcsec, approximately 10% of the SOFI detector field of view. This value was later increased to 70 arcsec for the November 2000 run to improve the background estimate. These offsets are constrained so that all distances between pointings, in a series of 15 consecutive pointings, are larger than 9 arcsec.

### 3. Data Reduction

#### 3.1. Image Processing

The infrared images were reduced using a new routine designed for the EIS pipeline for automated reduction of optical/infrared images (Vandame *et al.* 2001). The routine produces fully reduced images and weight-maps carrying out bias subtraction, flatfielding, de-fringing and subtraction of the background, first-order pixel-based image stacking (allowing for translation, rotation and stretching of the image) and astrometric calibration. De-fringing, sky-subtraction and elimination of image artifacts are done adopting a two-pass procedure: first, a preliminary image is obtained by stacking a set of sky-subtracted

frames, with the background estimated using a running median; second, objects are identified in this stacked image and masks are created; finally, the de-fringing/sky-subtraction step is repeated with the object masks mapped to the jittered position of each individual image. Deviant values are sigma-clipped and masked pixels are neglected. More details about the package will be presented when it is made publicly available (Vandame *et al.* 2001).

The primary reason for developing an entire new code was to improve on the photometric accuracy of faint objects which had been achieved in the earlier processing of the EIS-DEEP data. Further analysis of these data carried out by the EIS team and by other users (Cimatti 1999; see also the eclipse home page<sup>1</sup> and Devillard 1999 for more information) revealed a trend to underestimate the flux of objects, in some cases of  $\sim 0.2$  mag at faint magnitudes. Another important advantage of the new software package is that it produces weight-maps which are critical for the construction of image mosaics.

The effect of the two-step procedure is illustrated in Figure 2 which shows the sky-subtracted image obtained af-

<sup>1</sup> <http://www.eso.org/projects/aot/eclipse/>

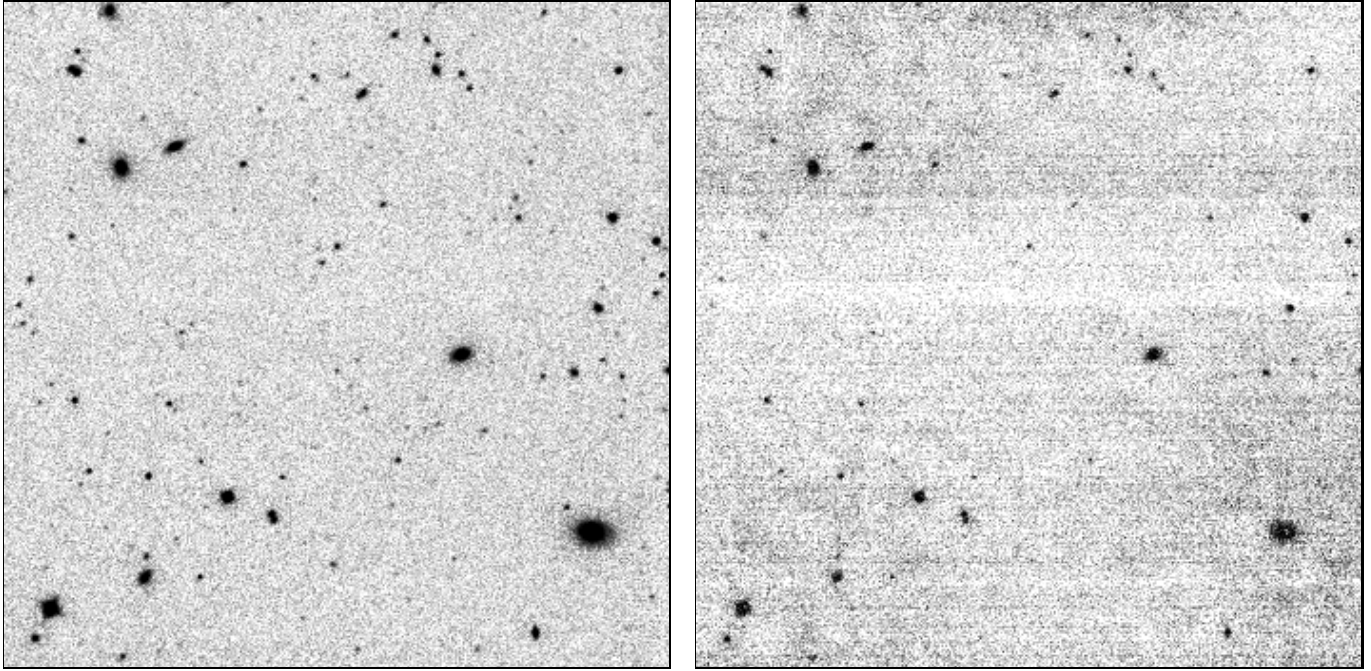


**Fig. 2.** Effect of the two-pass approach for the sky-estimation. The left panel shows the final sky-subtracted image (note the inverted fluxscale) after the second pass. The right panel shows the residuals after subtracting the first pass image from the second pass one. The large amounts of residual flux at the object positions indicate the necessity for the second pass background estimation.

ter the two-pass sky-estimation (left panel) and the residual after subtracting the first-pass image from the two-pass one (right panel). It can clearly be seen that a single pass leads to the loss of a significant fraction of flux leading to biases in the estimated magnitudes of up to  $\lesssim 0.3$  mag. This effect is caused by the biased sky-estimation in the outer regions of the objects where the faint light level contribution cannot be distinguished from the sky-background in the individual images. This effect is clearly visible in the lower right corner where the background around the bright galaxy is too high in the first pass estimate. Furthermore regions with a high density of individual faint sources, none of which can be detected prior to the final stacking, would contribute to the background in the single pass approach.

### 3.2. Astrometric Calibration

The astrometric calibration of the infrared frames was performed using as the reference catalog objects extracted from optical images obtained over the same region (Arnouts *et al.* 2001) using the method developed by Djamdji *et al.* (1993). The method is based on a multi-resolution decomposition of images using wavelet transforms (MVM) developed over the years by Bijaoui and collaborators and extensively applied in remote sensing. An implementation of these algorithms to stack images, referred to as MVM-astrometry, has been done for EIS. This package has proven to be efficient and robust for pipeline reductions. The estimated internal accuracy of this technique is about half a pixel ( $\sim 0.15$  arcsec). The optical images were calibrated relative to objects drawn from the pre-release version of the *Guide Star Catalog-II* (GSC-

II). The GSC-II (McLean *et al.* 2001) is based on multi-passbands all-sky photographic plate surveys including the Palomar Observatory Sky Survey (POSS-I-II), the SERC and the ESO Red Survey. The astrometric calibration of GSC-II has been obtained relative to Hipparcos (Perryman *et al.* 1997) and Tycho catalogs (Høg *et al.* 1997) and the *ACT* (Urban, Corbin & Wycoff 1998).

This two-step approach to astrometrically calibrate the infrared images has been taken for two main reasons. First, by using the deep astrometrically calibrated optical images as the reference the number of objects typically available within a SOFI field ( $\gtrsim 150$ ) is a factor of four larger than the typical number of GSC-II reference stars ( $\sim 40$ ). Therefore, this procedure provides a better constraint for a second-order polynomial fit. Second, this approach ensures a robust relative astrometry between the optical and infrared images, overcoming the problems identified in the earlier release of the CDF-S data. As pointed out by Benoist *et al.* (2001b) small relative shifts between the position of objects extracted from the optical and infrared images significantly affected the color catalog for that data set. The new procedure being adopted here should prevent similar problems from occurring in the future.

### 3.3. Photometric Calibration

The photometric calibration for each night is based on observations of standard stars taken from Persson *et al.* (1998). Typically two to seven stars were observed over a range of airmasses. For all nights independent photometric solutions were obtained with errors of  $\lesssim 0.03$  mag in both passbands and negligible color terms. Examining deviant measurements showed

that some of the selected standard stars (at least 3 cases) may be variable. A more careful analysis of these cases will be presented elsewhere.

Using the individually calibrated images, the consistency between their respective zero-points was examined considering the magnitude differences of pairs of objects located in regions of overlap. An average magnitude difference was then computed for each set of overlapping frames yielding a mean value of  $\sim 0.03$  mag and a scatter of  $\lesssim 0.09$  mag for both bands. A more detailed discussion of this point will be presented in a forthcoming paper when the complete data set has been analyzed and a final mosaic is created.

### 3.4. Image Products

The images being released are fully astrometrically (COE projection) and photometrically calibrated (normalized to 1 sec exposure time). The provided FITS files include both the pixel and weight maps as FITS extensions. The astrometric information is stored in the world coordinate system (WCS) keywords in the FITS headers. Similarly the photometric calibration is provided by the zero-point and its error available in the header keywords ZP and ZP\_ERR. The zero-point includes the normalized zero-point of the photometric solution and the atmospheric extinction correction. In the header one can also find a product identification number (P\_ID) which should always be used as reference. The headers also provide information on the number of stacked frames and the on-source total integration time. Additionally the seeing obtained by measuring the FWHM of bright stars in the final stacked images is stored in the header keyword SEE\_IMA.

An example of a final image and corresponding weight map is shown in figure 3 for one pointing in  $K_s$ . Note that the size of the image ( $\sim 5.8 \times 5.8$  square arcmin) is much larger than that obtained using the earlier version of the EIS pipeline which clipped the image to the best sampled region. Comparing the image and the weight map one sees how the noise increases at the edges as the effective exposure time decreases. However, proper use of the weight maps facilitates and greatly increases the efficiency of building up infrared mosaics.

It is worth mentioning that, a satellite track visible at the north-eastern corner in one of the  $J$ -band images (pointing (2,4)) led to the masking of a large region which caused the rejection of a large fraction of the frame from the final stack. Proper use of the Hough transform, as currently done for the optical images, will be used to correct this effect in future data products.

## 4. Source Lists

Source extraction was performed using the SExtractor software (Bertin & Arnouts 1996; ver. 2.2.1). Detection was carried out separately using the co-added image of each passband and field. The main parameters in the detection are the smoothing kernel, taken to be a Gaussian with a FWHM equal to 0.8 of that of the PSF measured on the frame; the SExtractor detection threshold, taken to be 0.8; and the minimum number of pixels

above the detection threshold, taken to be 7 pixels for SOFI images. As an illustration, the tabulation of the first 40 entries in one of the  $J$ -band source catalogs is presented in Table 3. All magnitudes are given in the  $AB$  system, using  $J_{AB} = J + 0.90$  and  $K_{AB} = K_s + 1.84$ . The table lists:

Column (1): the EIS identification name

Columns (2) and (3): right ascension and declination (J2000.0);

Columns (4)-(9): total, isophotal and aperture (3 arcsec diameter) magnitudes and respective errors. The first two magnitudes correspond to the `mag_auto` and `mag_iso` magnitudes measured by SExtractor. The magnitudes have been corrected for Galactic extinction taken from Schlegel *et al.* (1998). The errors are those estimated by SExtractor and include only the shot-noise of the measured source and background counts. Only objects detected with signal to noise  $S/N \geq 3$  (based on the isophotal magnitude errors) are included.

Column (10): an estimate of the  $S/N$  of the detection, by the inverse of the errors estimated for the isophotal magnitude;

Columns (11): the isophotal area  $A$  of the object in square arcsec;

Column (12): the half-light radius  $r_h$  in arcsec;

Column (13) and (14): minor to major-axis ratio and the position angle;

Column (15): the stellarity index computed by SExtractor;

Column (16): SExtractor flags (see Bertin 1998)

Column (17): EIS flags; these flags are used to identify objects in regions with very low weight or close to bright objects. Objects detected in regions with weight  $\geq 40\%$  of the maximum weight (proportional to the total integration time) and not affected by bright stars have EIS flag=0. Objects with weight  $< 40\%$ , located at the edges of the frame, have EIS flag=1. Finally EIS flag=2 indicates that the object is located in a region masked out due to the presence of a bright object.

Similar tables for each pointing and passband are available upon request in ASCII format. Catalogs for the mosaic and optical/infrared color catalogs will be distributed as soon as they become available. Note that besides distributing catalogs in tabular form as done here, catalogs in FITS formats will become part of the distribution of final products. These catalogs will include considerable more information such as the parameters defining the trimmed and masked regions used to determine the EIS flags. The final catalogs will be described by Arnouts *et al.* (2001).

## 5. Discussion

The characteristics of the data obtained by the present infrared survey are summarized in Table 4 which lists: in column (1) the identification of the pointing; in column (2) the filter; in column (3) the effective exposure time for each final image; in column (4) the seeing of the final co-added image; in column (5) the number of detected objects with  $S/N \geq 3$  as described above; in columns (6) and (7) the  $5\sigma$  and  $3\sigma$  limiting  $AB$  magnitude measured within an aperture  $2 \times \text{FWHM}$ . At the  $5\sigma$  limiting magnitudes the fraction of spurious objects is estimated to be  $\sim 5\%$  and  $\sim 11\%$  in  $J$  and  $K$ , respectively, rapidly rising to over 50% at the  $3\sigma$  limit. The fraction of spurious objects was

Table 3. CDF-S *J*-band source list (all magnitudes are given in the AB system).

#	$\alpha$	$\delta$	$m_{tot}$	$\epsilon$	$m_{iso}$	$\epsilon$	$m_{aper}$	$\epsilon$	$S/N$	$A$	$r_h$	$b/a$	$PA$	$class$	$Flag$	$EISflag$
EISJ033244.08-274048.6	03:32:44.08	-27:40:48.6	21.71	0.22	22.17	0.14	22.06	0.21	6.92	1.68	2.27	0.88	-10.45	0.90	24	1
EISJ033244.18-273942.3	03:32:44.18	-27:39:42.3	17.45	0.01	17.46	0.01	18.84	0.01	121.95	38.44	5.22	0.72	19.20	0.03	26	1
EISJ033244.20-273856.5	03:32:44.20	-27:38:56.5	22.04	0.23	22.49	0.22	22.23	0.53	4.49	0.50	0.66	0.82	46.70	0.92	16	1
EISJ033244.24-274111.0	03:32:44.24	-27:41:11.0	20.55	0.06	20.58	0.04	20.71	0.05	24.81	4.37	1.79	0.89	-3.05	0.98	16	1
EISJ033244.31-273953.9	03:32:44.31	-27:39:53.9	22.44	0.19	22.70	0.15	22.48	0.26	6.54	1.26	1.63	0.79	60.43	0.86	0	1
EISJ033244.33-273937.6	03:32:44.33	-27:39:37.6	20.23	0.05	20.29	0.04	20.54	0.04	25.06	5.55	2.15	0.87	43.58	0.97	19	1
EISJ033244.35-274036.4	03:32:44.35	-27:40:36.4	21.35	0.11	21.60	0.09	21.78	0.09	11.36	3.45	2.55	0.74	52.88	0.40	0	1
EISJ033244.42-274130.0	03:32:44.42	-27:41:30.0	22.14	0.26	23.24	0.19	22.85	0.26	5.33	0.93	3.27	0.74	38.08	0.67	0	1
EISJ033244.42-274422.4	03:32:44.42	-27:44:22.4	21.05	0.23	22.53	0.20	22.36	0.22	5.11	1.26	5.03	0.41	-25.72	0.93	0	1
EISJ033244.45-274108.4	03:32:44.45	-27:41:08.4	19.77	0.04	19.86	0.03	20.34	0.03	36.63	9.42	2.91	0.82	48.70	0.03	0	1
EISJ033244.48-274116.5	03:32:44.48	-27:41:16.5	22.20	0.17	22.37	0.12	22.45	0.19	8.23	1.93	2.14	0.62	-74.09	0.76	0	1
EISJ033244.52-274121.1	03:32:44.52	-27:41:21.1	22.10	0.16	22.30	0.12	22.26	0.17	8.38	2.19	2.14	0.88	32.19	0.92	0	1
EISJ033244.54-274221.6	03:32:44.54	-27:42:21.6	22.84	0.21	23.25	0.19	22.88	0.36	5.33	0.93	1.49	0.86	44.43	0.72	0	1
EISJ033244.56-273951.1	03:32:44.56	-27:39:51.1	22.45	0.19	22.76	0.16	22.51	0.25	6.30	1.35	1.69	0.82	-88.35	0.89	0	1
EISJ033244.63-273949.0	03:32:44.63	-27:39:49.0	21.53	0.17	22.08	0.10	22.11	0.13	9.67	2.44	2.90	0.78	-58.30	0.59	0	1
EISJ033244.65-274227.0	03:32:44.65	-27:42:27.0	22.88	0.20	23.24	0.16	22.92	0.32	6.12	0.84	1.40	0.70	0.67	0.56	0	1
EISJ033244.66-274202.7	03:32:44.66	-27:42:02.7	20.61	0.05	20.67	0.04	20.87	0.04	25.13	5.05	2.23	0.91	24.74	0.74	0	1
EISJ033244.67-274352.2	03:32:44.67	-27:43:52.2	21.95	0.19	22.64	0.15	22.52	0.18	6.76	1.60	2.55	0.74	30.18	0.90	0	1
EISJ033244.81-274406.7	03:32:44.81	-27:44:06.7	17.74	0.01	17.77	0.01	18.55	0.01	103.09	31.54	3.57	0.99	43.12	0.03	0	1
EISJ033244.94-274053.7	03:32:44.94	-27:40:53.7	22.85	0.32	23.58	0.22	22.92	0.30	4.47	0.76	1.83	0.85	18.15	0.61	0	1
EISJ033244.97-273915.8	03:32:44.97	-27:39:15.8	21.85	0.28	22.58	0.18	22.39	0.22	5.58	1.18	2.43	0.58	-72.83	0.91	0	1
EISJ033244.98-274309.5	03:32:44.98	-27:43:09.5	22.65	0.20	22.70	0.15	22.72	0.24	6.63	1.18	1.87	0.83	89.02	0.67	0	0
EISJ033245.04-274122.7	03:32:45.04	-27:41:22.7	22.04	0.14	22.10	0.10	22.08	0.15	10.46	1.93	1.70	0.88	-18.79	0.96	0	0
EISJ033245.06-274110.0	03:32:45.06	-27:41:10.0	19.89	0.05	20.01	0.03	20.86	0.03	29.85	11.69	4.18	0.58	-26.76	0.05	2	0
EISJ033245.06-274331.9	03:32:45.06	-27:43:31.9	18.35	0.01	18.35	0.01	19.20	0.01	94.34	30.36	3.75	0.92	54.48	0.03	0	0
EISJ033245.09-273913.7	03:32:45.09	-27:39:13.7	21.32	0.16	21.52	0.10	21.70	0.14	9.56	2.86	2.56	0.67	-60.67	0.70	0	0
EISJ033245.12-274256.1	03:32:45.12	-27:42:56.1	22.29	0.26	23.36	0.21	22.87	0.21	4.71	1.01	2.97	0.71	-68.73	0.53	0	0
EISJ033245.18-274147.5	03:32:45.18	-27:41:47.5	22.40	0.26	22.73	0.13	22.59	0.26	7.69	1.43	1.82	0.79	-46.23	0.92	0	0
EISJ033245.22-274058.0	03:32:45.22	-27:40:58.0	21.67	0.16	21.96	0.09	22.06	0.12	11.49	2.69	2.27	0.77	-1.86	0.57	0	0
EISJ033245.27-274052.1	03:32:45.27	-27:40:52.1	21.51	0.16	22.19	0.11	22.39	0.13	8.92	2.61	3.72	0.85	-59.45	0.02	1	0
EISJ033245.36-274249.8	03:32:45.36	-27:42:49.8	22.10	0.20	22.47	0.12	22.59	0.15	8.24	2.19	2.52	0.60	-25.28	0.39	0	0
EISJ033245.41-274225.6	03:32:45.41	-27:42:25.6	22.36	0.19	22.57	0.12	22.49	0.18	8.30	2.02	2.05	0.88	0.28	0.90	0	0
EISJ033245.41-274133.3	03:32:45.41	-27:41:33.3	21.17	0.08	21.32	0.06	21.55	0.07	16.78	4.21	2.41	0.84	20.64	0.63	0	0
EISJ033245.42-273923.2	03:32:45.42	-27:39:23.2	21.82	0.16	22.25	0.14	22.15	0.16	7.11	2.19	2.61	0.79	23.87	0.84	0	0
EISJ033245.43-274057.1	03:32:45.43	-27:40:57.1	20.94	0.10	21.32	0.06	21.63	0.07	16.31	4.37	3.25	0.87	56.58	0.44	3	0
EISJ033245.48-273915.5	03:32:45.48	-27:39:15.5	20.82	0.12	20.89	0.07	21.19	0.08	14.18	4.29	2.50	0.84	-81.82	0.78	2	0
EISJ033245.53-273913.7	03:32:45.53	-27:39:13.7	22.01	0.20	22.48	0.18	22.36	0.21	5.53	1.51	2.17	0.91	22.42	0.88	3	0
EISJ033245.53-274053.6	03:32:45.53	-27:40:53.6	19.68	0.04	19.82	0.03	20.58	0.02	39.22	13.88	3.91	0.83	28.41	0.03	3	0
EISJ033245.58-274114.4	03:32:45.58	-27:41:14.4	21.32	0.12	21.75	0.08	22.12	0.10	12.11	3.87	3.53	0.54	41.68	0.30	0	0
EISJ033245.58-274245.8	03:32:45.58	-27:42:45.8	22.42	0.16	22.50	0.11	22.51	0.19	9.26	1.93	1.71	0.89	-57.59	0.95	0	0

**Fig. 3.** An example of the final coadded image (left panel) and the corresponding weight map (right panel). The lines seen in the weight map are caused by the astrometric remapping of the frames.

**Table 4.** Data summary.

Pointing	filter	Eff.Exp.Time (sec)	Seeing (arcsec)	$N_{obj}$	$5\sigma_{lim}$ (mag)	$3\sigma_{lim}$ (mag)
(1,1)	$J$	3600	0.99	662	23.39	23.94
	$K_s$	4800	0.84	530	22.43	22.98
(1,2)	$J$	3600	0.77	736	23.48	24.03
	$K_s$	4800	0.76	795	22.54	23.09
(1,3)	$J$	3600	0.84	549	23.23	23.78
	$K_s$	4680	0.69	722	22.82	23.37
(1,4)	$J$	3600	0.77	871	23.59	24.14
	$K_s$	4500	0.77	663	22.64	23.19
(2,1)	$J$	3600	0.83	699	23.47	24.02
	$K_s$	4740	0.68	654	22.60	23.15
(2,4)	$J$	3600	0.82	534	23.02	23.57
	$K_s$	4800	0.81	566	22.43	22.98
(3,1)	$J$	3600	0.69	896	23.85	24.40
	$K_s$	4800	0.84	442	22.40	22.95
(3,4)	$J$	3600	0.87	697	23.47	24.02
	$K_s$	4800	0.77	602	22.62	23.17
(4,1)	$J$	3600	1.03	627	23.14	23.69
	$K_s$	4800	0.68	602	22.63	23.18
(4,2)	$J$	3720	0.86	588	23.38	23.93
	$K_s$	4920	0.85	415	22.37	22.92
(4,3)	$J$	3600	0.66	810	23.42	23.97
	$K_s$	7200	0.77	633	23.02	23.57
(4,4)	$K_s$	4800	0.67	710	22.71	23.26

estimated by creating catalogs from the survey images multiplied by  $-1$ . The mock images were then used as input to the catalog production and from the comparison between the catalogs of the mock and real objects the fraction of false-positives was estimated.

In order to externally verify the results obtained here the source list presented above was cross-correlated with that available from the 2MASS survey (Cutri *et al.* 2000) using a search radius of 1 arcsec. A total of 80 objects were found in common and their relative positions and magnitudes (for objects considered “good” in both catalogs) were computed and are shown in Figures 4 and 5. Apart from an offset of about 0.33 arcsec in right ascension one finds good agreement between the astrometric calibrations yielding a scatter of  $\lesssim 0.23$  arcsec. Assuming similar errors for both data sets one finds an astrometric accuracy of  $\sim 0.16$  arcsec consistent with the estimated internal accuracy of the technique adopted in the present work. The asymmetry of the distribution reflects a small systematic increase of the right ascension residuals noted near the eastern edge of the region. This effect is likely due to the large offset of the CDF-S position relative to the center of the original plate used for GSC-II object extraction. This problem is being addressed for the final release of the catalog. Considering objects brighter than  $J = 16.0$  and  $K_s = 15.0$  (Vega system), roughly corresponding to the 2MASS limiting magnitudes, the measured magnitudes of the two data sets are in good agreement, except for three outliers, showing a mean offset of 0.016 mag in

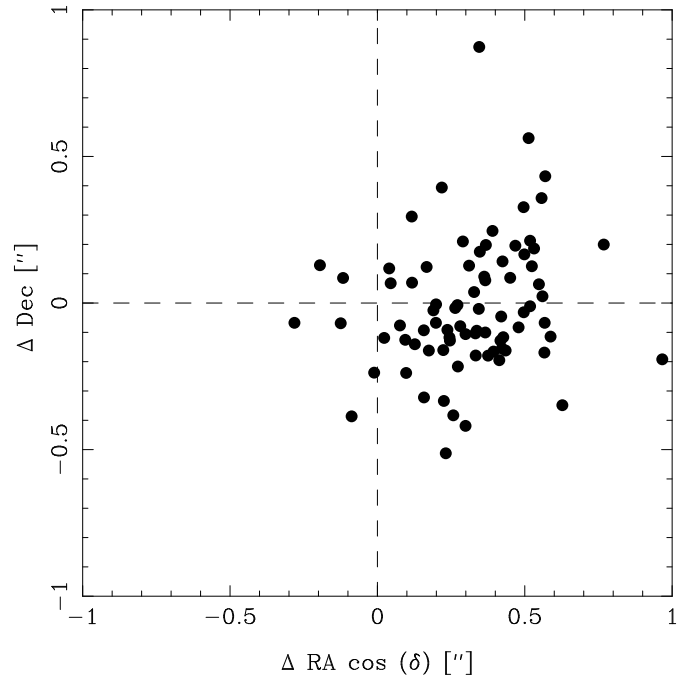


**Fig. 4.** Comparison between the location of objects in common with the 2MASS survey, offsets are computed as  $EIS - 2MASS$ .

$J$  and  $-0.031$  mag in  $K_s$ . The scatter is found to be 0.077 mag

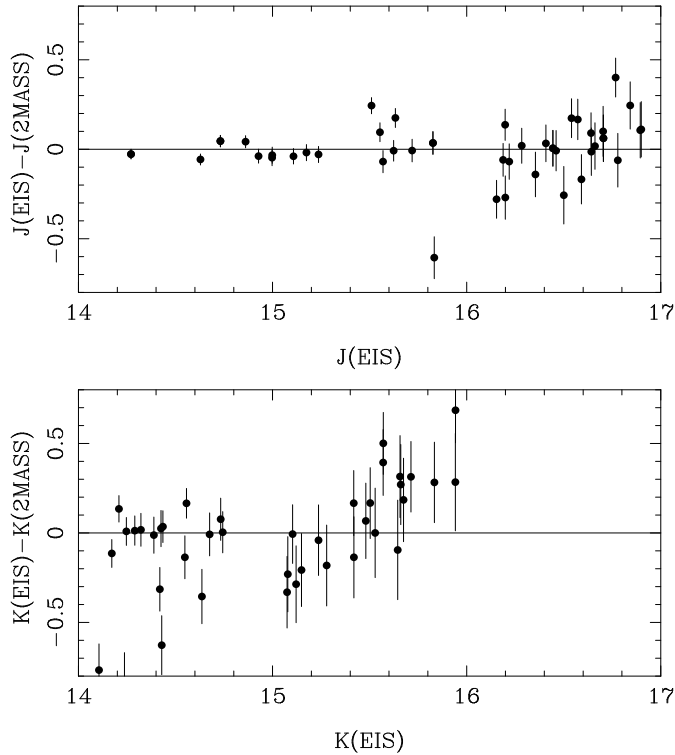


**Fig. 5.** Comparison between the measured  $J$  (upper panel) and  $K_s$  (lower panel) magnitudes of objects in common with the 2MASS survey.

and 0.14 mag, respectively, consistent with the estimated uncertainty of the overall zero-point (Section 3).

Finally, Figure 6 shows the comparison of galaxy counts as a function of the total magnitude with those obtained for other data sets. The derived slopes of the counts are  $0.33 \pm 0.02$  in  $J$  and  $0.35 \pm 0.02$  in  $K$ , in good agreement with those obtained by Saracco *et al.* (1999) as well as other studies. The galaxy counts shown in the figure is the mean counts obtained averaging all the individual catalogs and the error bar is the scatter. The individual catalogs were obtained drawing objects with stellarity index less than 0.95 or fainter than 20.5 mag and only including objects with  $S/N > 3$ . Bad objects were discarded based on the SExtractor and EIS flags.

## 6. Summary

This paper presents the first results of the infrared data accumulated by the ongoing Deep Public Survey being conducted by the EIS program. The paper describes the observations and the first set of products being publicly released including fully calibrated pixel maps and source lists covering the CDF-S region. Given the current interest in this area of the sky it was decided to release the data in the simple format presented. Other derived products will be described in forthcoming papers of this series. Hopefully, the source lists presented here will be of immediate value for cross-identification with X-ray sources.

*Acknowledgements.* The Guide Star Catalogue-II is produced by the Space Telescope Science Institute in collaboration with the Osservatorio Astronomico di Torino. Space Telescope Science

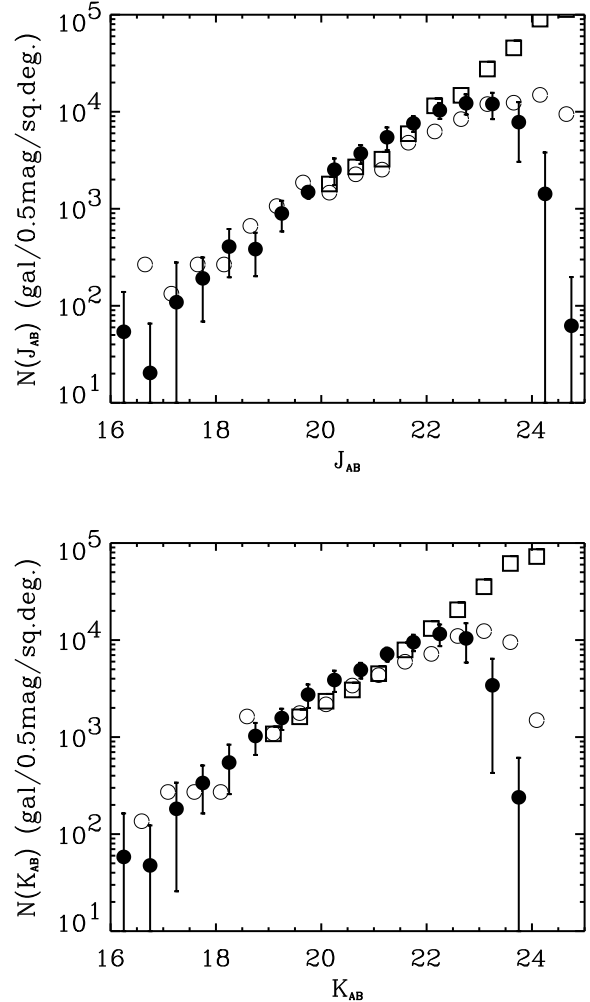


**Fig. 6.** Comparison of galaxy number counts between: the present work (full circles); da Costa *et al.* (1998) obtained from EIS-DEEP (open circles) and those of Saracco *et al.* (1999, squares).

Institute is operated by the Association of Universities for Research in Astronomy, for the National Aeronautics and Space Administration under contract NAS5-26555. Additional support is provided by the Association of Universities for Research in Astronomy, the Italian Council for Research in Astronomy, European Southern Observatory, Space telescope European Coordinating Facility, the International GEMINI project and the European Space Agency Astrophysics Division. The UK Schmidt Telescope was operated by the Royal Observatory Edinburgh, with funding from the UK Science and Engineering Research Council (later the UK Particle Physics and Astronomy Research Council), until 1988 June, and thereafter by the Anglo-Australian Observatory

This publication makes use of data products from the Two Micron All Sky Survey, which is a joint project of the University of Massachusetts and the Infrared Processing and Analysis Center/California Institute of Technology, funded by the National Aeronautics and Space Administration and the National Science Foundation.

We thank all of those directly or indirectly involved in the EIS effort. Our special thanks to M. Scodreggio for his continuing assistance in a variety of issues, A. Bijaoui for allowing us to use tools developed



by him and collaborators over the years and past EIS team members for building the foundations of this program. We would also like to thank A. Renzini and the members of the Working Group for Public Surveys.

## References

- Arnouts, S. *et al.* , 2001, In preparation  
Benoist, C. *et al.* , 2001a, In preparation  
Benoist, C. *et al.* , 2001b, In preparation  
Bertin, E. & Arnouts, S.; 1996, A&AS, 117, 393  
Bertin, E., 1998, SExtractor, User's guide, v2.0  
Cimatti, A, 1999, Private communication  
Cutri, R.M.; Skrutskie, M.F.; Van Dyk, S.; *et al.* , 2000, Explanatory Supplement to the 2MASS Second Incremental Data Release  
da Costa, L. *et al.* , 2001, In preparation  
da Costa, L. *et al.* , 1998, astro-ph/9812105, submitted to A&A  
Devillard, N., 1997, The Messenger, 87, 19  
Devillard, N, 1999, ADASS, 98, 333  
Djamdjji, J.P.; Bijaoui, A. & Manière, R.; 1993, Photogrammetric Engineering and Remote Sensing, 59, 645  
Giacconi, R; Rosati, P.; Tozzi, P.; *et al.* , 2000, astro-ph/0007240, submitted to ApJ  
Høg, E.; Bässgen, G.; Bastian, U.; *et al.* , 1997, A&A, 323, L57  
McLean, B.; Greene, G.; Lattanzi, M.; *et al.* , 2001, in Mining the Sky, Proc. of ESO Workshop, Springer-Verlag, In press  
Moorwood, A.; Cuby, J.G.; & Lidman, C.; 1998, The Messenger, 91,9  
Perryman, M. A. C.; Lindegren, L.; Kovalevsky, J.; *et al.* , 1997, A&A, 323, L49  
Rengelink, R. *et al.* , 1998, astro-ph/9812190, submitted to A&A  
Renzini, A. & da Costa, A., 1997, The Messenger, 87, 23  
Saracco, P.; D'Odorico, S.; Moorwood, A.; *et al.* , 1999, A&A, 349, 751  
Schlegel, D.; Finkbeiner, D. & Davis, M.; 1998, ApJ, 500, 525  
Urban, S. E.; Corbin, T. E. & Wycoff, G. L., 1998 AJ 115, 2161  
Vandame, B. *et al.* , 2001b, In preparation

This figure "deep2c\_nosusi\_BW.jpg" is available in "jpg" format from:

<http://arxiv.org/ps/astro-ph/0102300v2>

This figure "k-img.jpg" is available in "jpg" format from:

<http://arxiv.org/ps/astro-ph/0102300v2>

This figure "k-weight.jpg" is available in "jpg" format from:

<http://arxiv.org/ps/astro-ph/0102300v2>